# Influence of anti-ageing compounds on rheological properties of bitumen

Gao, Yangming; Zhang, Yuqing; Omairey, Eman L.; Al-Malaika, Sahar; Sheena, Husam

**DOI**
10.1016/j.jclepro.2021.128559

**Publication date**
2021

**Document Version**
Accepted author manuscript

**Published in**
Journal of Cleaner Production

**Citation (APA)**
Gao, Y., Zhang, Y., Omairey, E. L., Al-Malaika, S., & Sheena, H. (2021). Influence of anti-ageing compounds on rheological properties of bitumen. *Journal of Cleaner Production*, *318*, Article 128559. https://doi.org/10.1016/j.jclepro.2021.128559

# Influence of anti-ageing compounds on rheological properties of bitumen

Yangming Gao[a, b], Yuqing Zhang[c*], Eman L. Omairey[c], Sahar Al-Malaika[a], and Husam Sheena[a]

[a]Polymer Processing and Performance (PPP) Research Unit, Department of Chemical Engineering and Applied Chemistry (CEAC), Aston University, Aston Triangle, Birmingham B4 7ET, UK

[b]Section of Pavement Engineering, Faculty of Civil Engineering & Geosciences, Delft University of Technology, Stevinweg 1, 2628 CN, Delft, The Netherlands

[c]Department of Civil Engineering, Aston University, Aston Triangle, Birmingham B4 7ET, UK

* Corresponding Author (y.zhang10@aston.ac.uk)

## Abstract:

The aim of this study was to investigate the effects of different anti-ageing compounds (AACs) on the oxidative stability, rheological and mechanical properties of bitumen. Modified bitumen samples containing six different AAC combinations, with five samples containing Irganox acid (3,5-di-tert-butyl-4-hydoxyphenylpropionic acid), a hindered phenol polymer-based antioxidant, were fabricated and aged under different conditions using a Rolling Thin Film Oven (RTFO) as well as a Pressure Aging Vessel (PAV). The oxidative stabilising performance (anti-ageing) of the AACs was examined using Fourier Transform Infrared (FTIR) Spectroscopy. The effect of the AAC-modified bitumen on different rheological and mechanical properties was investigated - complex viscosity, linear viscoelastic (LVE) properties, fatigue and rutting - using a Dynamic Shear Rheometer (DSR). The results illustrated that all the AAC-combinations examined afforded good oxidative stability to the base bitumen, with outstanding anti-ageing performance achieved by formulations C, D, E and F (Irganox acid:NaMMT, Irganox acid:furfural without or with DLTDP or NaMMT). The rheological results showed that the AAC-modified bitumen samples displayed non-Newtonian characteristics associated with simple thermo-rheological materials. The AAC formulations A (DLTDP:furfural), D (Irganox acid:furfural) and F (DLTDP:Irganox acid:furfural) were shown to significantly strengthen the resistance of the bitumen samples to fatigue cracking. In contrast to Irganox acid:furfural combination, the addition of the NaMMT nanofiller to this mixture was found to enhance the rutting resistance of the aged bitumen samples.

**Keywords:** Bitumen; Anti-ageing compounds; Rheological properties; Fatigue cracking; Rutting resistance

## 1. Introduction

Bitumen is a complex hydrocarbon produced from refining petroleum. When mixed and compacted with the graded mineral aggregates, the bitumen acts as a binder to fabricate asphalt mixtures used for paving the road surfaces. The bitumen is known to undergo oxidative ageing which leads to severe stiffness and brittleness of bitumen-based asphalt products in-service. Inherently, therefore, oxidation is one of the main processes that contribute to the chemical instability of bitumen in-service; water and other factors, e.g., volatilization, polymerization, syneresis and thixotropy, contribute considerably also to the loss of the adhesive attributes of the bitumen in asphalt products (Apeagyei, 2011; Gao et al., 2018; Omairey et al., 2021). The oxidative ageing of bitumen, which occurs throughout the service life of asphalt pavements, is caused by a complex set of irreversible chemical reactions in the bitumen initiated by atmospheric oxygen causing changes in its molecular structure leading to a build-up of carbonyl and sulfoxide functional groups (Petersen and Glaser, 2011; Petersen and Harnsberger, 1998).

A correlation was found between the bitumen's hardening susceptibility and the carbonyl content (Glover et al., 2009). Thus, the oxidative ageing of bitumen can be quantified by the extent of build-up of the carbonyl functional groups. Researchers have developed different ways to evaluate the growth of the carbonyl functional groups using Fourier Transformation Infrared (FTIR) Spectroscopy (Hou et al., 2018). Carbonyl area (CA) is a parameter defined as the integral area within a wavelength range from 1820 to 1650 $cm^{-1}$ under an absorbance curve from the FTIR test (Cui et al., 2018). Although the CA was widely used to characterise the ageing performance of the bitumen, it was shown that the fixed wavelength range (1820-1650 $cm^{-1}$) used for this parameter can lead to an inaccuracy in the CA calculation when the bitumen does not contain all the carbonyl functional groups determined from FTIR under this specific wavenumber range prior to ageing (Omairey et al., 2019). Herrington (2012) measured the normalized carbonyl area under the spectra from 1640 to 1810 $cm^{-1}$ for variations in sample concentration (using a baseline at 1810 $cm^{-1}$). To eliminate the effect of FTIR sample thickness, Liu et al. (2015) proposed a carbonyl index (CI) that was defined as the ratio of carbonyl area (under the peak at 1700 $cm^{-1}$) to the area of methylene group (under the peak at 1375 $cm^{-1}$).

The build-up of various oxidation products (such as carbonyl and sulfoxides) causes an increase in the molecular size and cohesive energy density and a decrease of the fraction of the free volume which would eventually lead to the hardening of the bitumen (Gao, 2020; Gao et al., 2019). The age-hardening of bitumen has a detrimental effect on the durability of asphalt pavements as this would increase the susceptibility of the asphalt pavements to cracking leading to premature failure of pavements. In order to prolong the service life of asphalt pavements, research efforts have been made in which different anti-ageing compounds (AACs) have been used to reduce the bitumen's oxidative hardening (Apeagyei, 2006; Apeagyei, 2011; Gawel et al., 2016; Karnati et al., 2019; Omairey et al., 2019; Xu et al., 2017). Xu et al. (2017) used FTIR to investigate the anti-ageing performance of asphalt binder modified by wood lignin and found that the lignin improved the ageing resistance of asphalt binder through resisting the formation of carbonyl structure during the ageing process. Karnati et al. (2019) employed silica nanoparticles (SNPs) functionalised with (3-aminopropyl) triethoxysilane (APTES) to enhance the ageing resistance of asphalt binder. Ding et al. (2019) applied a mixed solvent of heptane and trichloroethylene (TCE) to dissolve and extract recycled asphalt shingle (RAS) binder. Results indicated that the extracted RAS presented a good anti-aging performance. Omairey et al. (2019) developed a screening method to select potential AACs to combat the oxidative degradation of bitumen. They had used a normalized carbonyl index (NCI) to quantify the oxidative ageing of the AAC-modified bitumen and to evaluate the anti-ageing (stabilising) effectiveness of different compound types using FTIR. It was found that the samples containing AACs based on furfural:DLTDP, Irganox acid (10-15%), Irganox acid:sodium montmorillonite (NaMMT), and furfural had exhibited a high anti-ageing performance. Although the work of Omairey et al. (2020) had reported a preliminarily set of results on the resistance to fatigue cracking of some AAC-modified bitumen samples, a more comprehensive investigation of other potential AAC formulations on the rheological and mechanical properties are further investigated here.

The main objective of this study was therefore to investigate the effects of some anti-ageing compounds (AACs) on the anti-ageing performance, rheological and mechanical properties of the AAC-modified bitumen. Six AACs (five of which containing Irganox acid, both alone and in combination with other compounds) were evaluated after fabrication in base bitumen (40/60). All the AAC-modified bitumen samples, which were aged (using a Rolling Thin Film Oven, RTFO, and a Pressure Aging Vessel, PAV), were evaluated for their effect on the oxidative stabilising (anti-ageing) performance (using FTIR spectroscopy) and rheological and mechanical behaviour (using Dynamic Shear heometry, DSR) with respect to the complex viscosity, linear viscoelastic (LVE) properties, fatigue and rutting performance of the bitumen formulations.

## 2. Materials and method

### 2.1 Materials and preparation of modified bitumen

A type of base bitumen with a penetration grade of 40/60 was used as a control binder for all the tests. The base bitumen 40/60 has been employed to measure the effectiveness of anti-ageing additives (AACs) in the authors' previous study (Omairey et al., 2019). Only one type of bitumen was examined in this study in order to eliminate the binder-source effects (Omairey et al., 2019; Yao et al., 2013b; You et al., 2011). The anti-ageing compounds (AACs) were selected based on the work by Omairey et al. (2019). All the AACs used were commercial compounds except for Irganox acid which was synthesised in our laboratories as a precursor for polymer antioxidant (Dintcheva et al., 2015). A list of the AACs formulations and their concentrations used in this study are summarised in **Table 1**. Dilauryl thiodipropionate (DLTDP) is typically used as a secondary antioxidant in polymers. Furfural is an organic aldehyde. Irganox acid was synthesised by the following procedure: 1) a suspension of Irganox 1076 in a solution of methanol/water (MeOH/$H_2O$) and sodium methoxide (MeONa) was refluxed under $N_2$ atmosphere; 2) the side product (stearyl alcohol) was removed from the resulting mixture; and 3) the Irganox acid in the form of a white powder was obtained by washing with water and drying the product. The synthesised Irganox acid is a hindered phenol typically used as a precursor for hindered phenol-based antioxidants. Sodium montmorillonite (NaMMT) is an inorganic nano-clay nanomaterial usually used as an additive to improve the resistance against permanent deformations of bitumen. The chemical structures and physical characteristics of these additives are shown in **Table 2**.

**Table 1** Anti-ageing compounds (AACs) and their concentrations used in the bitumen.

| ID | Anti-ageing compounds (AACs) | Concentration (% by weight of bitumen) |
|---|---|---|
| A | (3:4) DLTDP (Dilauryl thiodipropionate):furfural | 3.5% |
| B | Irganox acid | 10% |
| C | (3:2) Sodium montmorillonite (NaMMT):Irganox acid | 25% |
| D | (2:1) Irganox acid:furfural | 15% |
| E | (3:2:1) NaMMT:Irganox acid:furfural | 12% |
| F | (2:2:1) DLTDP:Irganox acid:furfural | 10% |

The AAC-modified bitumen samples were fabricated in the laboratory by mixing the AACs with the base bitumen. The AACs formulations are presented in **Table 1**. For example, sample A comprises DLTDP (1.5% by weight of base bitumen) and furfural (2%). A high-speed shear mixer was used to blend the control bitumen and the AACs with the specific concentrations given in **Table 1**. The mixing was conducted at 150 ℃ for 30 min and a shear speed of 500 rpm. After mixing, the modified sample was slowly poured from the beaker to the container and its flow was observed to identify the dispersion of the ingredients. For all modified samples, no block was seen in the samples, which indicates the ingredients were completely dispersed in the base bitumen. This proved that the blending conditions including the temperature, time and speed are suitable for different modified samples. It is noted that the control sample (i.e., base bitumen) was also subjected to the same blending process in order to ensure that all the samples underwent the same blend-induced ageing condition.

All control and modified bitumen samples were initially aged using a Rolling Thin Film Oven (RTFO) at 163 ℃ for 85 min (ASTM, 2012) to simulate the short-term ageing of the samples during the field mixing and compaction stage of asphalt pavement construction. The RTFO aging was followed by further ageing in a Pressure Aging Vessel (PAV) at 100 ℃ with air blow of 2.1 MPa (ASTM, 2013); to simulate different levels of ageing, the PAV testing was conducted over 10 and 20 hours.

**Table 2** Chemical and physical characteristics of additives used in this study.

| Name | Identity | State | Melting point (℃) | Solubility in water (% w/w) | Chemical structure |
|---|---|---|---|---|---|
| DLTDP | organic thioester | solid (white flakes) | 39-42 | < 0.01 | 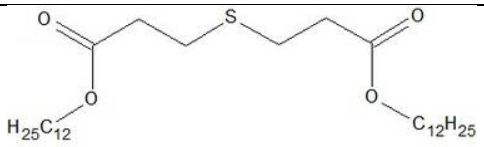 |
| Furfural | organic aldehyde | liquid | -38 | 7.4 | 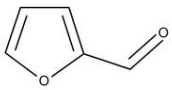 |
| Irganox acid | hindered phenol | solid (white crystals) | 50-55 | < 0.01 | 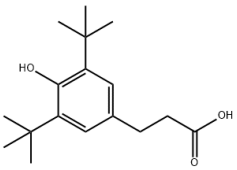 |
| NaMMT | inorganic clay nanomaterial | solid (yellow powder) | none | insoluble | 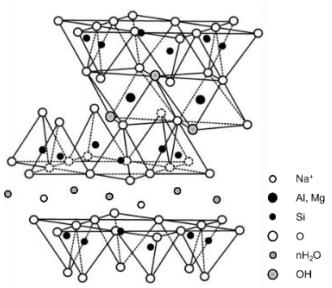 |

## 2.2 Fourier transform infrared (FTIR) spectroscopy test

Fourier transform infrared (FTIR) spectroscopy tests were conducted for all the unaged and aged bitumen samples to measure the oxidative transformation and in particular the changes in the carbonyl functional groups in these samples due to ageing. The AAC-modified bitumen was cast as a thin film (0.5 mm thickness) by dissolving (at room temperature) in a small amount of dichloromethane used as a solvent here due to its high bitumen dissolving ability followed by complete evaporation of the solvent under nitrogen (Lamontagne et al., 2001; Omairey et al., 2019). The thin-film samples were then placed on a sodium chloride disc in an infra-red cell holder. FTIR spectral measurements were carried out using a Perkin-Elmer spectrum 100 instrument (resolution 4 $cm^{-1}$, 32 scans, range 450-4000 $cm^{-1}$), as shown in **Fig. 1(a)**. Background scans were run first before scanning the samples, and all FTIR measurements were carried out in duplicates. **Fig. 2** shows a representative transmission FTIR spectrum of the base bitumen.

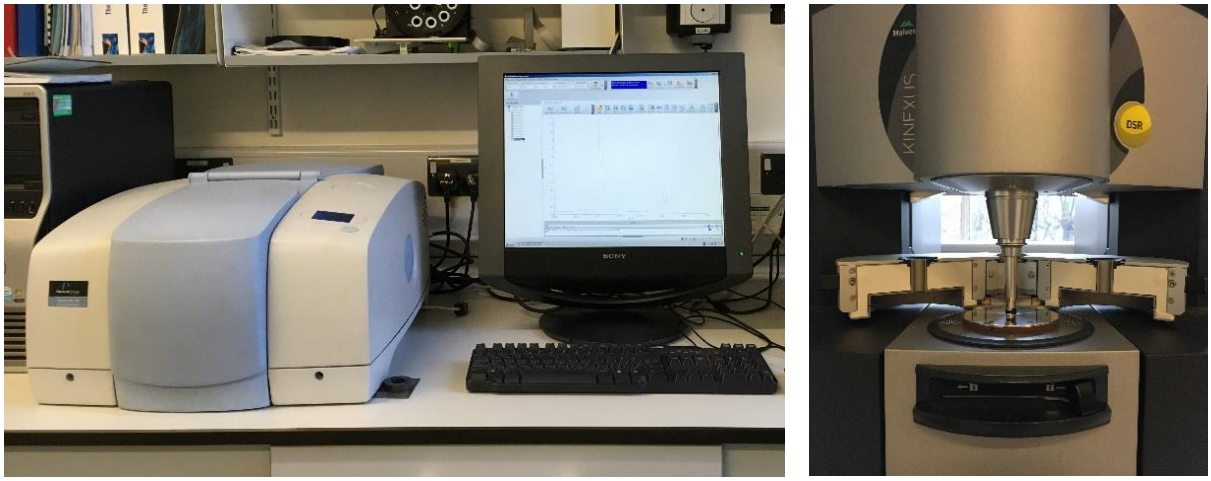

(a) FTIR (b) DSR

**Fig. 1.** Instruments used in this study.

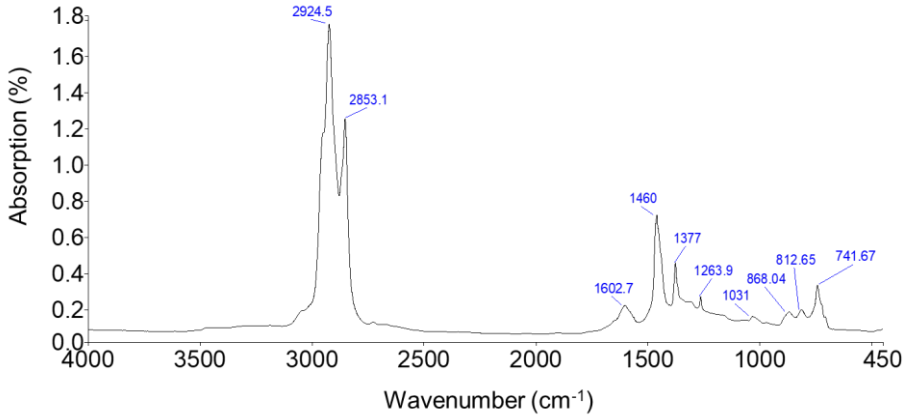


**Fig. 2.** FTIR spectrum of the unaged control bitumen sample 40/60.

2.3 Dynamic shear rheometer (DSR) tests

Dynamic shear rheometer (DSR) tests were conducted to evaluate the rheological and mechanical properties of the bitumen samples using a Kinexus Rheometer from Malvern Panalytical shown in **Fig. 1(b)**. A silicone mould was used to prepare the test samples with a diameter of 8 mm (2 mm in height) or 25 mm (1 mm in height). A series of DSR tests including frequency sweep test, time sweep fatigue test and multiple stress creep recovery (MSCR) test were conducted on unaged and aged bitumen samples. **Table 3** illustrates the testing schemes used in this study.

**Table 3** Testing schemes used in this study.

| NO | Test method | Purpose | Test parameters | Bitumen tested |
|---|---|---|---|---|
| 1 | RTFO | Short term ageing | 163 ℃, 85min | Unaged |
| 2 | PAV | Long term ageing | 100 ℃, 2.1MPa, 10h, 20h | RTFO aged |
| 3 | FTIR | Anti-ageing evaluation | Room temperature | All samples |
| 4 | Frequency sweep | Viscosity/Stiffness | 20, 30, 40, 50 and 60 ℃ | Unaged & PAV aged |
| 5 | Time sweep | Fatigue | 20 ℃, 10Hz, 5% strain | PAV aged |
| 6 | MSCR | Rutting | 64 ℃ | RTFO aged |

Note: RTFO, Rolling Thin Film Oven; PAV, Pressure Ageing Vessel; LVE, Linear Viscoelastic; and MSCR, Multiple Stress Creep and Recovery.

166

167 *2.3.1 Frequency sweep test*

168 Frequency sweep test was used to measure the linear viscoelastic (LVE) properties of the bitumen samples.
169 The tests were conducted on the unaged and 20-hour PAV aged samples from 0.1 to 25 Hz over a
170 temperature range of 20 ℃ ~ 60 ℃ with an increment of 10 ℃ to obtain the samples' complex shear
171 modulus, phase angle and complex viscosity. To ensure that the frequency sweep tests were run within
172 the LVE response of the materials, strain amplitude sweep tests were undertaken with the strain
173 amplitudes ranging from 0.1% to 30% to identify the LVE region and measure the damage tolerance of
174 different samples prior to the frequency sweep tests. **Fig. 3** presents an example for the results of
175 frequency sweep tests of the bitumen samples.

176

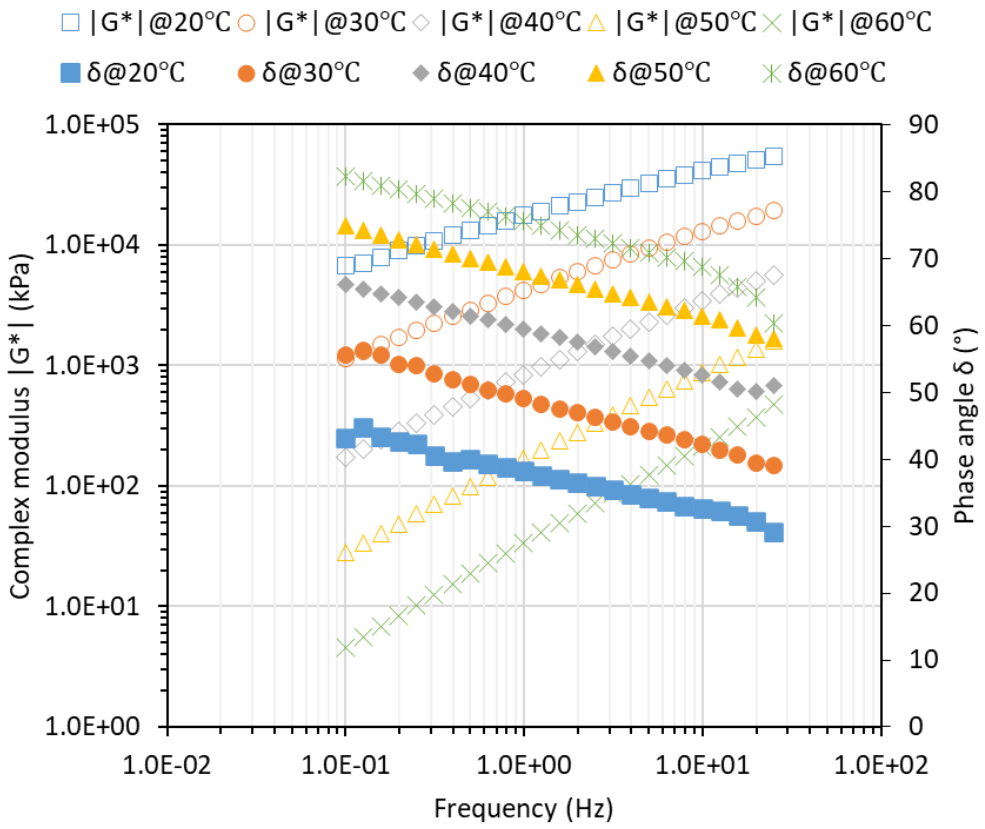


177

178 **Fig. 3.** Results of frequency sweep tests of the 20-hour PAV aged control bitumen sample 40/60.

179

180 *2.3.2 Time sweep test*

181 Time sweep test was performed to evaluate the fatigue performance of the 20-hour PAV aged bitumen
182 samples at an intermediate temperature. The parallel loading plates with 8 mm diameter (2 mm gap) were
183 used in this test. The tests with a 5% strain amplitude were carried out at temperature of 20 ℃ and
184 frequency of 10 Hz for 40 min (i.e., 24,000 load cycles) to determine the complex shear moduli and phase
185 angles of the samples in the damaged condition. **Fig. 4** illustrates an example for the results of time sweep
186 tests of the bitumen sample.

187

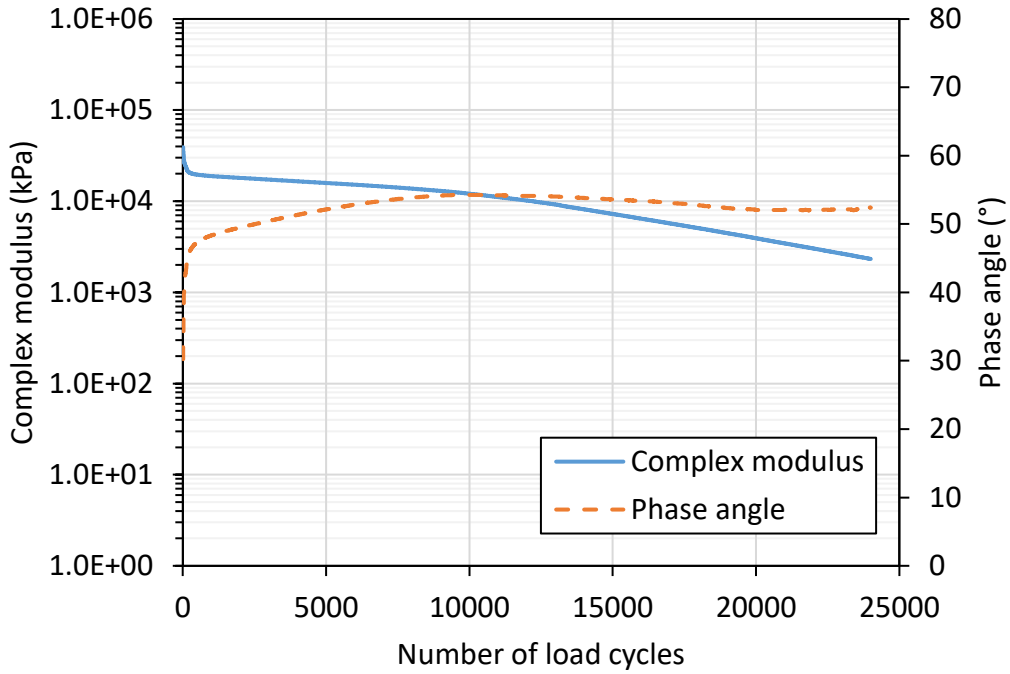


**Fig. 4.** Results of time sweep tests of the 20-hour PAV aged control bitumen sample 40/60.

*2.3.3 Multiple stress creep and recovery (MSCR) test*

Multiple stress creep and recovery (MSCR) test was used to measure of the rutting performance of different bitumen samples at elevated temperatures (ASTM, 2010); the loading plates used in this test were disc-shapes of 25 mm diameter × 1 mm . The MSCR tests were performed on the RTFO aged samples at temperature of 64 ℃ to obtain the non-recoverable creep compliance and the percent recoverable strain of the samples. In this test, the samples were loaded at a constant stress level for 1s and then allowed to recover for 9s. Following twenty creep and recovery cycles at 0.1 kPa creep stress, ten creep and recovery cycles were run at 3.2 kPa creep stress.

## 3. Results and discussion

3.1 Evaluation of AACs' stabilising effectiveness in bitumen after ageing

Prior to analysing the rheological properties of the AAC-modified bitumen samples, the stabilising (anti-ageing) performance of the AACs was evaluated based on FTIR test results (conducted in duplicates) for unaged, RTFO aged, 10-hour and 20-hour PAV aged samples by measuring the changes in the carbonyl-forming oxidation products with ageing. **Fig. 5** shows the carbonyl region, where the build-up of the main oxidation products are expected to appear, in the infrared spectra of the AAC-modified bitumen, in this case it is shown for the 20-hour PAV aged bitumen sample modified by the formulation A (DLTDP:furfural).

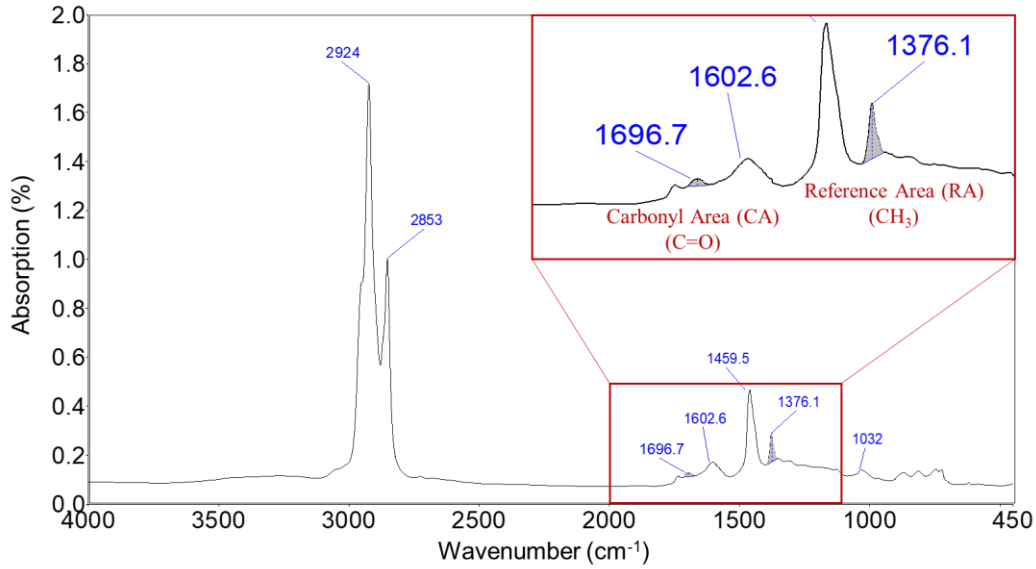


**Fig. 5.** FTIR spectrum of the bitumen sample modified by the formulation A (DLTDP:furfural) after 20-hour PAV ageing.

A normalized carbonyl index (NCI) is used to quantify the samples' oxidative ageing performance. NCI is defined as the ratio of the difference between the carbonyl index at any ageing time ($CI_t$) and the carbonyl index before ageing at time zero ($CI_0$) to that of the initial carbonyl index $CI_0$, as shown in **Eq. (1)**; the carbonyl index (CI) is calculated according to **Eq. (2)**. CI is the ratio of the areas under the C=O region with a peak around 1700 $cm^{-1}$ to that of a reference $CH_3$ peak around 1377 $cm^{-1}$; the reference peak is assumed to be unaffected by ageing and hence allows one to compensate for differences in sample thickness and the effect of changes in the film thickness on ageing. In this study, the two-point method was used to calculate the peak areas. The baseline was created by connecting the lower and upper limits on the two sides of the peak in the spectrum curve, as shown in **Fig. 5**.

$$NCI = \frac{CI_t - CI_0}{CI_0} \quad (1)$$

$$CI = \frac{CA}{RA} \quad (2)$$

where *NCI* is the normalized carbonyl index; $CI_t$ is the carbonyl index for the samples with different ageing times (i.e., unaged, RTFO aged, 10-hour PAV aged and 20-hour PAV aged); $CI_0$ is the initial carbonyl index for the unaged samples; *CA* is the carbonyl area centred around 1700 $cm^{-1}$; and *RA* is the reference area centred around 1377 $cm^{-1}$.

**Fig. 6** shows the NCI values with different ageing regimes and times for all the tested bitumen samples. It can be seen that all the modified samples with the AACs have lower values of NCI compared to that of the control bitumen sample 40/60 thus all the six AAC formulations used in this study tend to improve the oxidative ageing of the bitumen. It is interesting to note that all the samples containing Irganox acid, except that of sample EB (NaMMT:Irganox acid:furfural modified bitumen), show a negative NCI value under all ageing regimes tested here, which contrasts to the behaviour of the non-Irganox acid containing sample AB (DLTDP:furfural modified bitumen) and sample E (NaMMT:furfural:Irganox acid modified bitumen) where their NCI increases sharply after the 10-hour and 20-hour PAV ageing, see **Fig. 6**. It is important to point out here that while the unaged bitumen modified with DLTDP:furfural, sample AB, has no significant absorption in the carbonyl region, see **Fig. 7(a)**, all the unaged samples containing Irganox acid show a significant absorption in this region which is due to the carboxylic acid carbonyl absorption peak centred around 1710 $cm^{-1}$ characteristic of Irganox acid itself, see **Fig. 7(b)** (bitumen

containing Irganox acid, sample BB) and **inset**, **Fig. 7(c)** (Irganox acid, (Omairey et al., 2019)). It is clear from **Fig. 6** that all the samples containing Irganox acid, except for sample EB, show an excellent stabilising performance and in excess of that afforded by the AAC combination DLTDP:furfural (sample AB). The reason for the negative carbonyl index observed after the PAV ageing for the Irganox acid-containing samples (samples BB, CB, DB and FB) is attributable to the sacrificial loss of Irganox acid with ageing (see **Fig. 8** as an example) as a result of its mode of action as an antioxidant (as evidenced from the decrease in the intensity of its characteristic carboxylic acid function, & the decrease of NCI during ageing**,** see **Fig. 6**) in preventing the oxidation of bitumen.

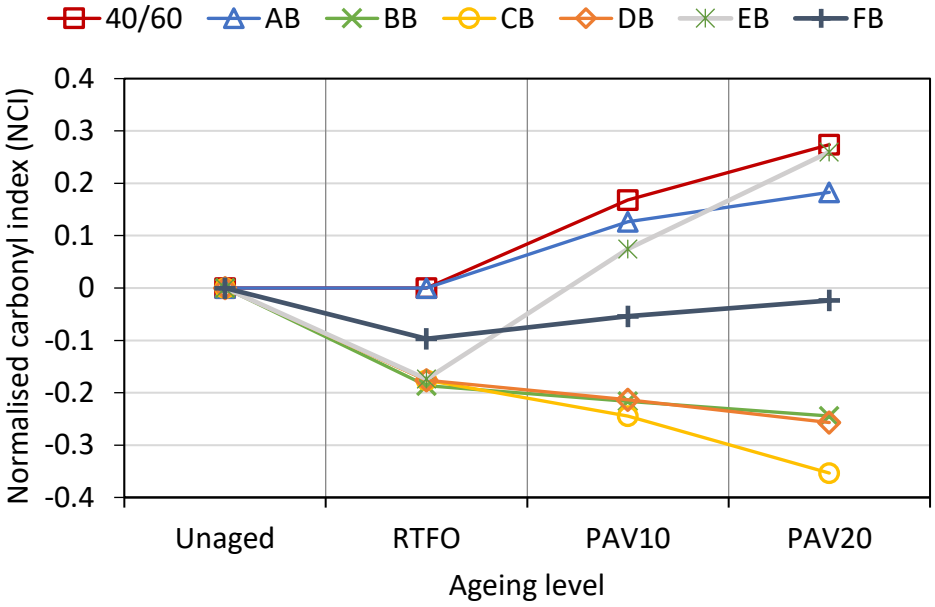


**Fig. 6.** Normalized carbonyl index (NCI) with different ageing levels for all the bitumen samples. (Note: in the legend, the first letter stands for the ID of AACs shown in Table 1 and the second one is the initial letter of the word 'Bitumen'. For example, AB means the bitumen sample modified by the additive A. In the horizontal axis, PAV10 and PAV20 stand for 10-hour PAV and 20-hour PAV ageing levels, respectively.)

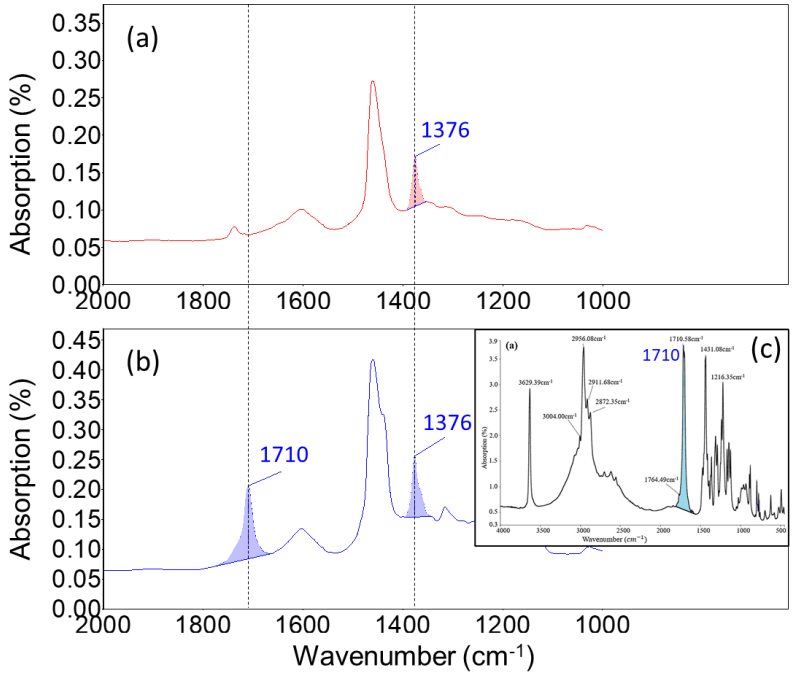

**Fig. 7.** FTIR spectra in the region 2000-1000 $cm^{-1}$ of (a) unaged bitumen containing DLTDP:furfural (sample AB) and (b) unaged bitumen containing Irganox acid (sample BB). (c) The inset in (b) is the FTIR spectral region of Irganox acid showing its carboxylic carbonyl absorption at 1710 $cm^{-1}$.

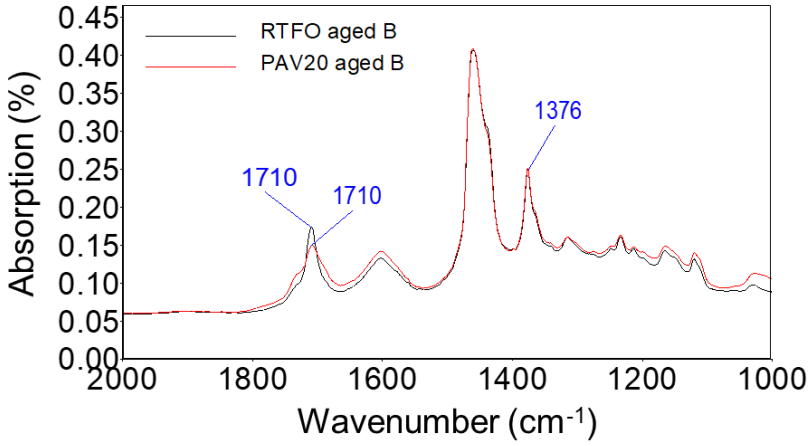


**Fig. 8.** FTIR spectra in the region 2000-1000 $cm^{-1}$ of RTFO and 20-hour PAV aged bitumens containing Irganox acid (sample BB).

It should be noted here that although sample EB (NaMMT:Irganox acid:furfural modified bitumen) shows a negative NCI after RTFO ageing (**Fig. 6**), its NCI value shows a substantial increase after the PAV ageing at both 10 h and 20 h. This suggests that furfural is affecting negatively the oxidative stability of the bitumen substrate, and may be acting antagonistically with the Irganox acid in the presence of the NaMMT. This suggestion is supported by the fact that both samples DB (furfural:Irganox acid modified bitumen) without NaMMT, and CB (NaMMT:Irganox acid modified bitumen) without furfural, have shown very effective stabilisation which is clearly illustrated by the sacrificial loss of the Irgamox acid (and reduction in its carbonyl signature on ageing, hence the negative NCI observed) in affording protection to the bitumen. Clearly, furfural is an ineffective AAC when compared to that of the other AAC candidates investigated here. Moreover, the fact that the addition of Irganox acid to the same combination of DLTDP:furfural (i.e. F, DLTDP:Irganox acid:furfural) results in a considerably enhanced stabilising performance when compared to that shown by the combination DLTDP:furfural (A) is a further support to the above suggestion about the negative stabilising effect of furfural.

### 3.2 Effect of AACs on complex viscosity of bitumen

The complex shear viscosity of all the unaged bitumen samples was obtained from the frequency sweep tests at different temperature, as shown in **Fig. 9**. **Fig. 9(a)** illustrates the complex viscosity versus the frequency at the temperature of 40 °C. It can be seen that the viscosity is dependent on the frequency, which decreases with increasing frequency (shear rate). At 40 °C, the control bitumen sample 40/60 and all the AAC-modified samples exhibit non-Newtonian (shear thinning) behaviour since the viscosity decreases as the shear rate increases. **Fig. 9(b)** shows the complex viscosity versus temperature at a frequency of 0.1 Hz. It is found that the viscosity decreases as the temperature increases, which indicates the viscosity is also dependent on the temperature.

It can be seen also from **Fig. 9** that samples BB (containing Irganox acid) and CB (the combination Irganox acid:NaMMT modified bitumen) have a slightly greater complex viscosity than the control bitumen sample 40/60. This is because that they contain a high concentration (10%) of Irganox acid. However, the bitumen sample modified by Irganox acid:furfural (DB) show a lower viscosity than that of the control sample due to the low viscosity liquid-nature of the furfural. The effect of furfural on the

complex viscosity is further supported by the lower viscosity of samples AB (DLTDP:furfural modified bitumen) and EB (NaMMT:Irganox acid:furfural modified bitumen). Thus, it is concluded that the Irganox acid enhances the complex viscosity of the samples while the furfural can be used to reduce the viscosity. The sample modified by DLTDP:Irganox acid:furfural (FB) has a smaller viscosity than the control sample (40/60 bitumen) at different temperatures (except 60 ℃) and frequencies. It is noted that the polymer network of this formulation DLTDP:Irganox acid:furfural can be formed by cross-linking of molecular chains of the ingredients within the bitumen matrix. Thus, a weak polymer network of FB sample reduces its complex viscosity due to the presence of furfural (liquid) in the combination DLTDP:Irganox acid:furfural. However, at the temperature of 60 ℃, the complex viscosity of FB sample is slightly larger than that of the control sample, indicating that the network of FB sample enhances its complex viscosity at higher temperature (i.e., 60 ℃). The temperature of 60 ℃ has exceeded the melting points of DLTDP (39-42 ℃) and Irganox acid (50-55 ℃) shown in **Table 2**. Therefore, DLTDP with long molecular hydrocarbon chains, Irganox acid and furfural in bitumen matrix form a strong crosslinking and/or entanglement, leading to an increase in complex viscosity of FB sample.

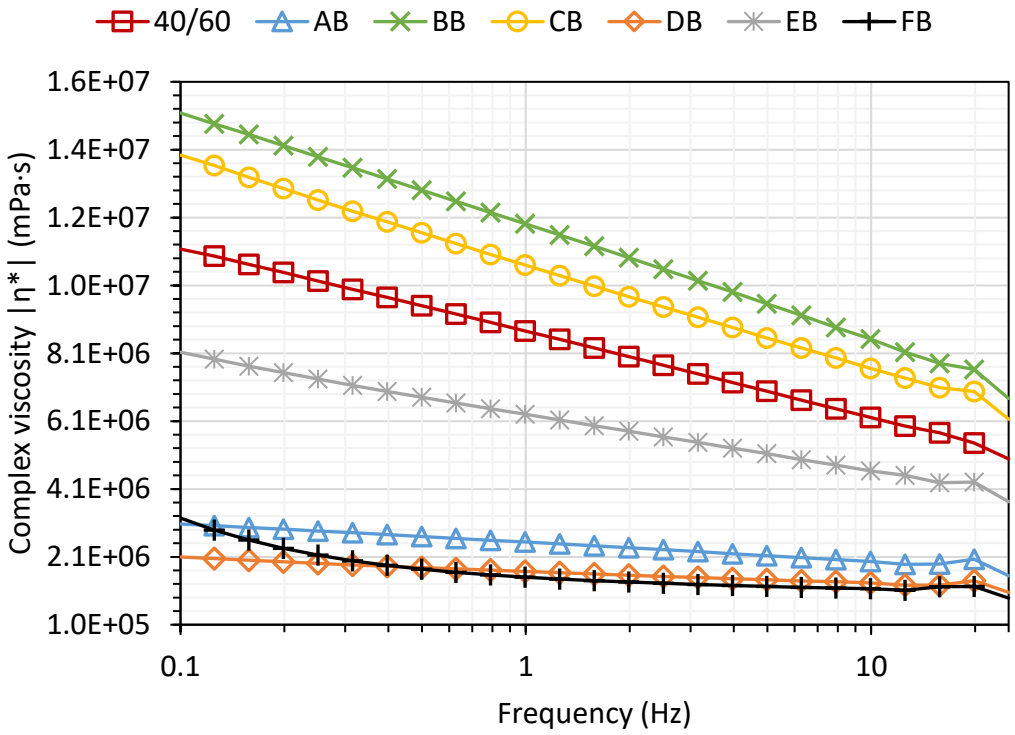


(a) Complex viscosity versus frequency at 40 ℃

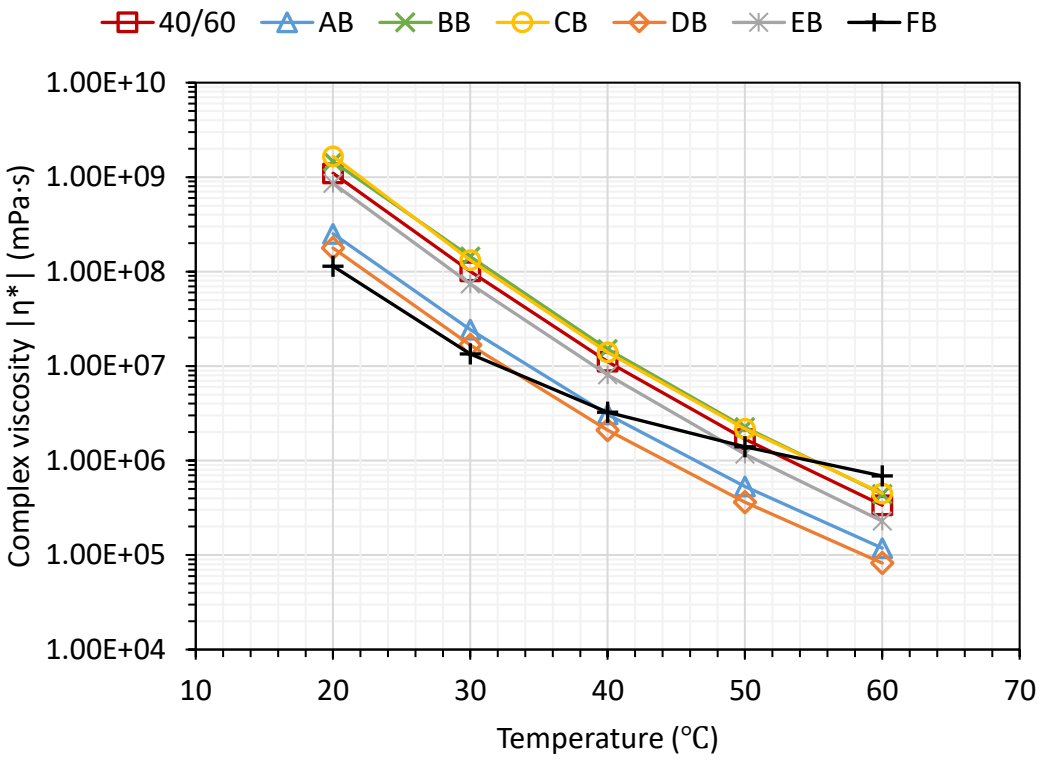


(b) Complex viscosity versus temperature at 0.1 Hz

**Fig. 9.** Complex viscosity of all the unaged samples versus (a) frequency at 40 ℃ and (b) temperature at 0.1 Hz.

## 3.3 Complex modulus and phase angle of the modified bitumen

### *3.3.1 Black diagram*

A black diagram is a graph of the complex modulus versus the phase angle obtained from the frequency sweep tests at different temperatures. In the black diagram, the frequency and the temperature are eliminated, which allows the viscoelastic properties of the bitumen to be analysed without performing the time-temperature superposition principle (TTSP) manipulations of the raw dynamic data. A smooth curve in the black diagram indicates the time-temperature equivalency. The black diagram has been widely used to identify possible errors in the measurements, thermo-rheological simplicity of the samples, and different types of binders (Airey, 2002; Wang et al., 2018).

The black diagrams of all the bitumen samples at the unaged and 20-hour PAV aged conditions are shown in **Fig. 10**. It is seen that the dynamic data of all the samples present a relatively smooth trend. This indicates that the unaged and aged samples can be considered as thermo-rheologically simple materials. The black diagrams of all the unaged samples are shown in **Fig. 10(a)**. In the black diagram, the curves of samples AB, BB, CB, DB and EB have a trend similar to that of the control sample 40/60. These curves are overlapping in black space. However, the curve of the sample FB exhibits an inverse ‘‘C’’ pattern, which is significantly different from that of the control sample. This inverse ‘‘C’’ pattern was also reported in the literature for the SBS modified bitumen (Airey, 2002; Wang et al., 2018). At the low temperature (i.e., 20 ℃), the sample FB has a behaviour similar to that of the control sample as the linear viscoelastic response is mainly dominated by the bitumen phase (Cuciniello et al., 2020). At the higher temperatures (i.e., 30 to 60 ℃), the curve of the sample FB tends towards lower phase angles. The trend may be caused by the polymer network of the combination F (DLTDP:Irganox acid:furfural) formed by

cross-linking of molecular chains of its ingredients within the bitumen matrix, which resists viscous flow and controls the rheological response at higher temperatures.

**Fig. 10(b)** illustrates the black diagrams of all the 20-hour PAV aged samples. Laboratory aging affects the viscoelastic response of the samples. Compared to the unaged dynamic data shown in **Fig. 10(a)**, it can be seen that the black diagrams at the aged condition shift towards the left (a lower phase angle) for the samples 40/60, AB, BB, CB, DB and EB, which means these 20-hour PAV aged samples have more elastic behaviour. At the low temperatures (i.e., 20 and 30 ℃), the same trend can be found for the sample FB. However, at the higher temperatures (i.e., 50 and 60 ℃), the black diagram of the aged sample FB tends towards a greater phase angle (right), which indicates more viscous behaviours. This could result from the viscoelastic response being mainly dominated by the bitumen phase at the high temperatures due to the sacrificial loss of the combination F (DLTDP:Irganox acid:furfural) after 20-hour PAV ageing. This phenomenon was also observed in other works (Airey and Brown, 1998; Cuciniello et al., 2020). Thus, the curve of the aged sample FB has a trend similar to that of the remaining samples rather than an inverse ‘‘C’’ pattern at the unaged condition. These curves of all the samples are overlapping in the black diagram, as shown in **Fig. 10(b)**.

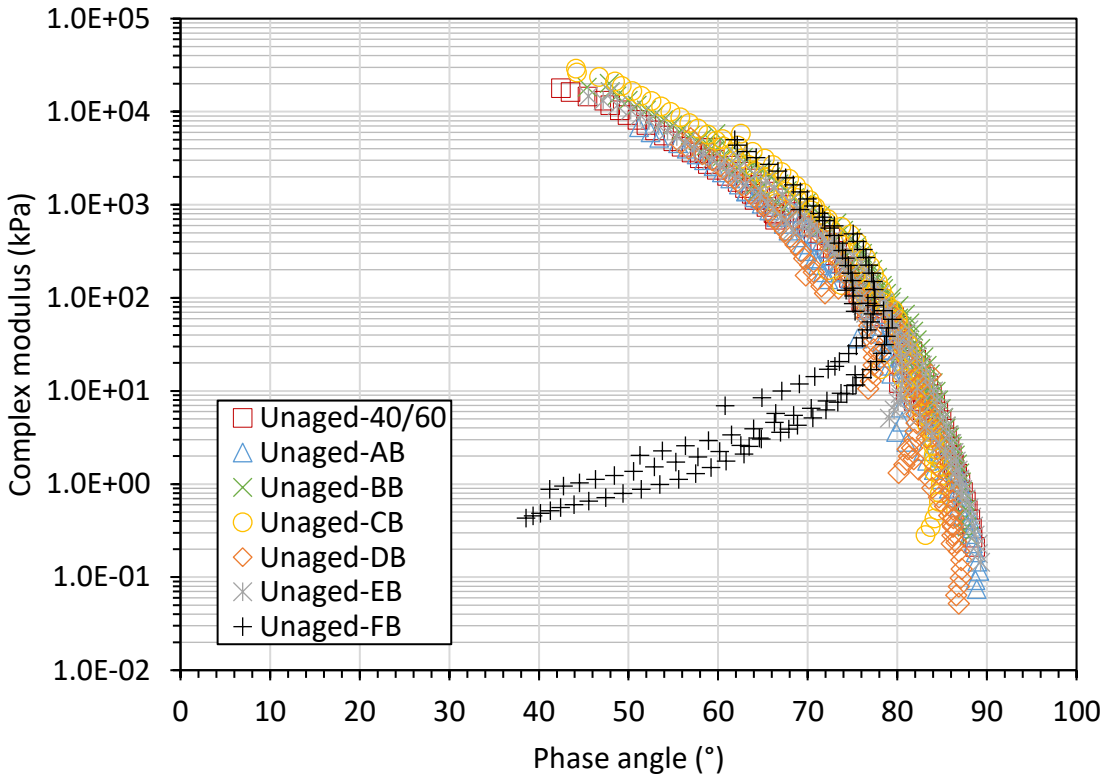


(a) Black diagrams for the unaged samples

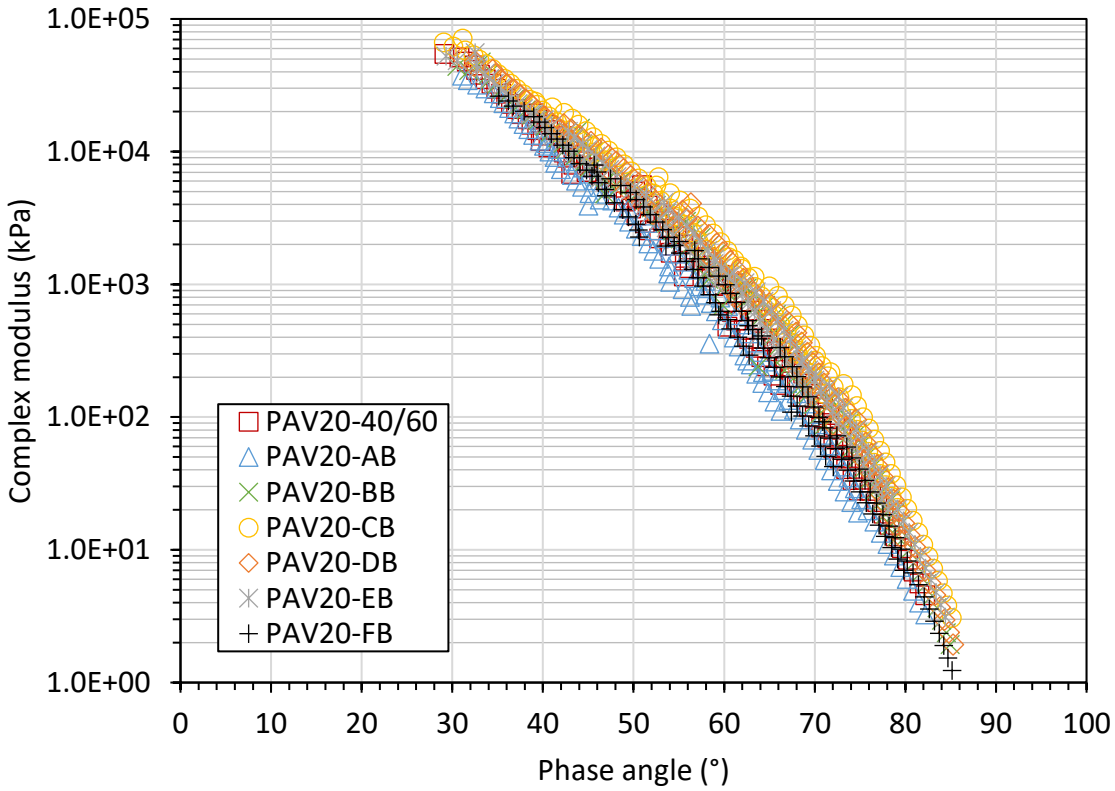


(b) Black diagrams for the 20-hour PAV (PAV20) aged samples

**Fig. 10.** Black diagrams of all the samples at (a) unaged and (b) 20-hour PAV aged conditions.

*3.3.2 Master curve*

Master curve has been widely employed to investigate the stiffness (flow) properties of bitumen samples over a wide range of frequency and temperature (Tang et al., 2018; Wang et al., 2018; Yusoff et al., 2013). Based on the measured dynamic data (i.e., complex modulus and phase angle) at different temperatures and loading frequencies, the master curves can be constructed at a reference temperature using the TTSP. In this study, the master curve of complex modulus is developed using the sigmoidal model expressed in **Eq. (3)** (Tang et al., 2018; Yusoff et al., 2013; Zhang et al., 2016).

$$\log|G^*| = \nu + \frac{\alpha}{1+e^{\beta+\gamma\log(f_r)}} \quad (3)$$

where $|G^*|$ is complex modulus; $\nu$ is the lower asymptote; $\alpha$ is the difference between the values of the upper and lower asymptotes; $\beta$ and $\gamma$ are the shape parameters; and $f_r$ is the reduced frequency that can be obtained by the loading frequency $f$ × the time-temperature shift factor $\alpha_T$.

**Fig. 11** shows the master curves of complex modulus for all the unaged and 20-hour PAV aged bitumen samples at the reference temperature of 40 °C. The complex modulus for all the samples increases with the increasing reduced frequency at the unaged and aged conditions. It is found from **Fig. 11 (a)** that the addition of the additives B (Irganox acid) and C (NaMMT:Irganox acid) leads to a slight increase in the complex modulus of the samples at the unaged condition. This means that the samples BB and CB are a little stiffer than the control sample 40/60 due to the presence of a high concentration (10%) of Irganox acid. However, the samples AB, DB, EB and FB containing the furfural exhibit a lower complex modulus than the control sample, indicating that they become softer because of the addition of the furfural.

Compared to the unaged samples, all the 20-hour PAV aged samples have a greater complex modulus, as shown in **Fig. 11 (b)**. The master curves of all the samples (except for the sample FB) are close to that of the control sample 40/60 at the aged condition, which demonstrates that the stiffness of these aged samples is not significantly changed by the AACs, resulted from the sacrificial loss of the additives after 20-hour PAV ageing. It is noted that the complex modulus of the aged sample FB is much smaller than that of the aged control sample. This indicates that the addition of the formulation F (DLTDP:Irganox acid:furfural) makes the bitumen softer at the aged condition.

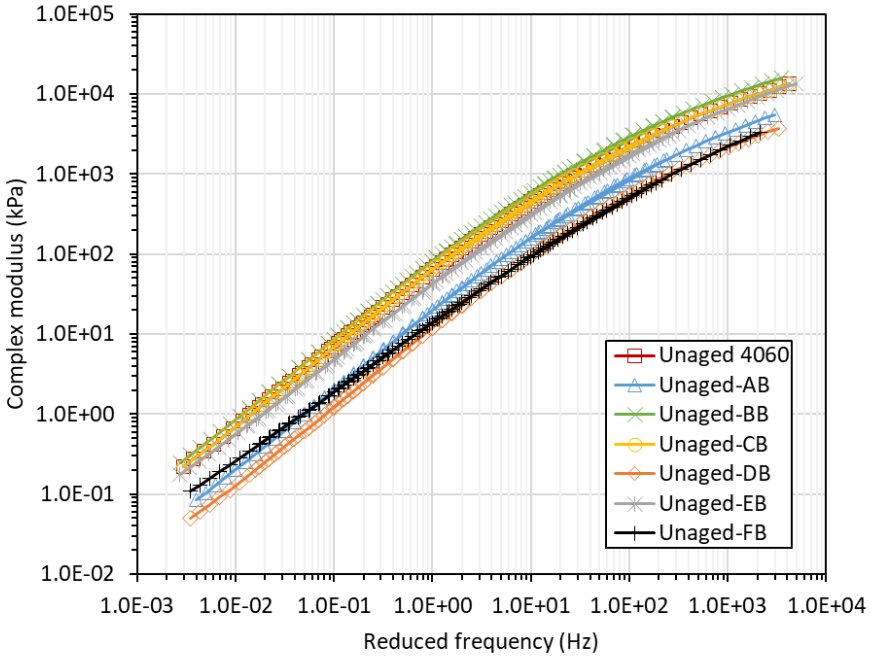


(a) Master curves for the unaged samples

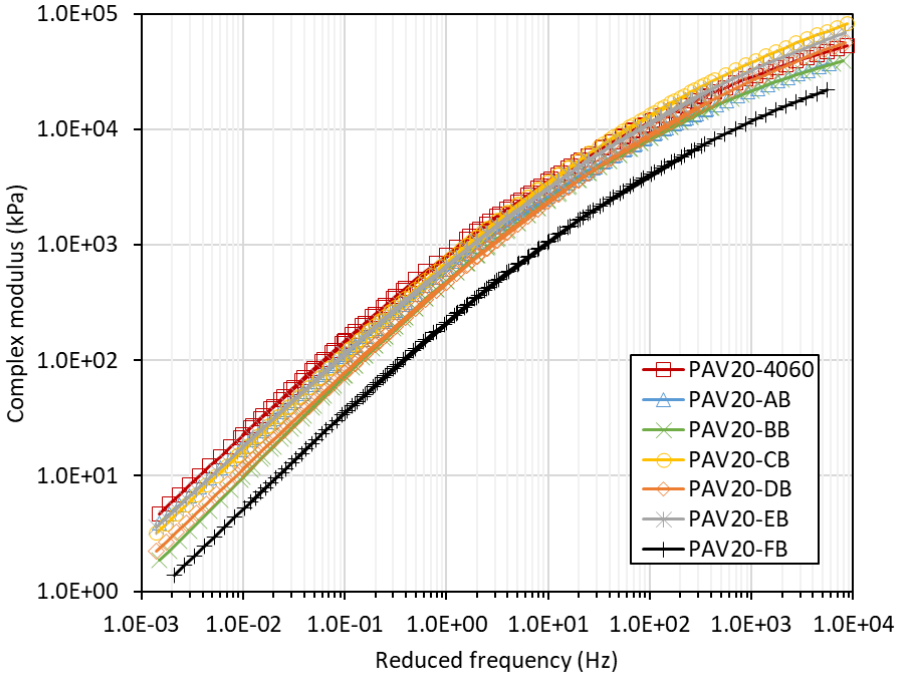


(b) Master curves for the 20-hour PAV (PAV20) aged samples

**Fig. 11.** Master curves of complex modulus for all the samples at (a) unaged and (b) 20-hour PAV aged conditions.

### 3.4 Effect of AACs on fatigue performance of bitumen

The fatigue resistance potential of the 20-hour PAV aged bitumen samples at the intermediate temperature (20 ℃) is evaluated using a DSR-based cracking (DSR-C) model developed by the authors based on damage mechanics in the previous work (Gao et al., 2020a, b; Li et al., 2020; Zhang and Gao, 2019). In the DSR-C model, the crack length in the bitumen during a time weep fatigue test is predicted by the samples' shear moduli and phase angles in the undamaged and damaged conditions, as shown in **Eq. (4)**. The shear modulus ($|G_0^*|$) and the phase angle ($\delta_0$) in the undamaged condition were obtained from the frequency sweep tests. The shear modulus ($|G_N^*|$) and the phase angle ($\delta_N$) at the *N*th load cycle in the damaged condition were recorded up to 24,000 load cycles in the time sweep tests. It is noted that the fatigue crack length predicted from the DSR-C model has been validated by comparing with the measured crack length using a digital visualisation approach for unmodified and modified bitumen at different temperatures, frequencies and strain levels in the previous work (Zhang and Gao, 2019).

$$c = \left[1 - \left(\frac{|G_N^*| / \sin(\delta_N)}{|G_0^*| / \sin(\delta_0)}\right)^{\frac{1}{4}}\right] r_0 \quad (4)$$

where $c$ is the crack length in the cylindrical bitumen sample; $r_0$ is the original radius of the bitumen sample; $|G_0^*|$ and $\delta_0$ are the shear modulus and the phase angle in the undamaged condition, respectively; and $|G_N^*|$ and $\delta_N$ are the shear modulus and the phase angle at the *N*th load cycle in the damaged condition, respectively.

The crack length in the bitumen was calculated at the 24,000$^{th}$ load cycle for all the 20-hour PAV aged samples using the DSR-C model in **Eq. (4)** to evaluate their fatigue performance, as shown in **Fig. 12**. It is seen that the crack length values of the samples AB (1.95 mm) and FB (1.98 mm) are smaller than that of the control sample 40/60 (2.24 mm). This indicates that the addition of the formulations A and F containing DLTDP and furfural can enhance the resistance of the bitumen to fatigue cracking, which agrees well with the findings reported in the literature (Omairey et al., 2020). In contrast, the samples BB and CB present greater crack length (2.60 mm and 2.48 mm) than the control sample, which means that the fatigue resistance of the bitumen is weakened by the additives B (Irganox acid) and C (NaMMT:Irganox acid). Compared to the sample BB containing Irganox acid, the sample DB with Irganox acid:furfural has a lower crack length (2.05 mm), indicating that furfural improves the fatigue performance of the bitumen modified by the additive B (Irganox acid). However, the furfural becomes ineffective in the fatigue improvement due to the addition of NaMMT, which is demonstrated by the higher crack length (3.04 mm) of the sample EB with NaMMT:Irganox acid:furfural. In conclusion, among the six types of the anti-ageing compounds, A (DLTDP:furfural), D (Irganox acid:furfural) and F (DLTDP:Irganox acid:furfural) can significantly strengthen the fatigue performance of the bitumen samples.

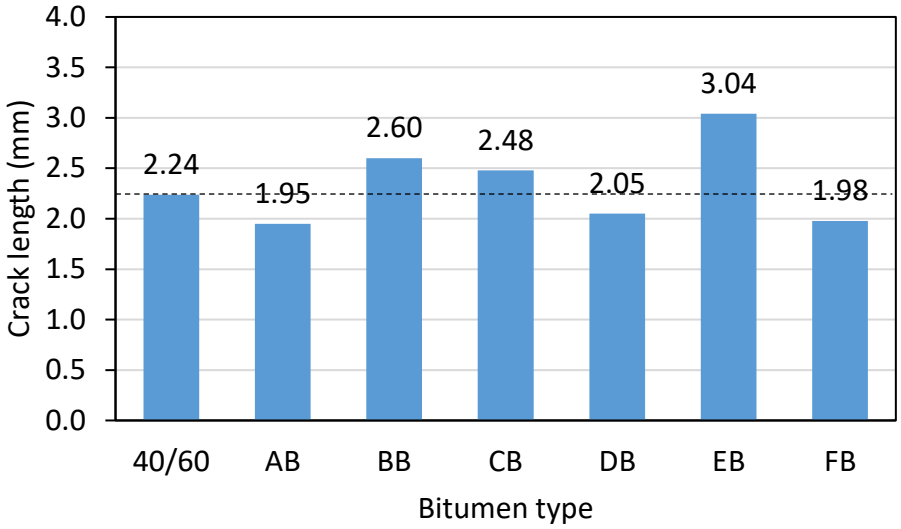


**Fig. 12.** Fatigue crack length calculated for all the 20-hour PAV aged samples.

3.5 Effect of AACs on rutting performance of bitumen

The rutting resistance potential of the RTFO aged bitumen samples at the high temperature is evaluated by the non-recoverable creep compliance and the percent recoverable strain that can be obtained by **Eqs. (5)** and **(6)** based on the results from the MSCR tests. The non-recoverable creep compliance and the percent recoverable strain are employed to characterise the deformation resistance and the elastic property of bitumen samples, respectively. A smaller non-recoverable creep compliance with a higher percent recoverable strain is desirable, which means a better resistance to rutting for the bitumen at the high temperature.

$$J_{nr} = \frac{\varepsilon_{nr}}{\sigma} \tag{5}$$

where $J_{nr}$ is non-recoverable creep compliance ($kPa^{-1}$), $\varepsilon_{nr}$ is non-recoverable strain at end of rest period of 9 s, and $\sigma$ is stress level (kPa) applied during creep phase.

$$\varepsilon_r = \frac{\varepsilon_1 - \varepsilon_{10}}{\varepsilon_1} \times 100\% \tag{6}$$

where $\varepsilon_{nr}$ is percent recoverable strain, $\varepsilon_1$ is strain at the end of 1 s creep phase, and $\varepsilon_{10}$ is strain at the end of 10 s creep phase.

**Fig. 13** illustrates the MSCR parameters (i.e., the non-recoverable creep compliance and the percent recoverable strain) for all the RTFO aged bitumen samples. It can be seen that the MSCR parameters of sample AB are close to that of the control sample 40/60, which means that the rutting performance of the bitumen is not significantly changed by the formulation A (DLTDP:furfural). However, the sample FB shows the highest non-recoverable creep compliance with the lowest percent recoverable strain due to the presence of Irganox acid. The sample BB with the additive Irganox acid also has a higher non-recoverable creep compliance with a lower percent recoverable strain than that of the control sample. This demonstrates that the addition of Irganox acid reduces the rutting resistance of the samples. Compared to the sample BB, the MSCR parameters of the samples DB and CB indicates that the furfural weakens its rutting performance while the NaMMT strengthens its rutting resistance, respectively. The role of NaMMT in improving the rutting performance is also found by the MSCR parameter comparison of the samples DB and EB. This finding is consistent with the previous research on the effects of the nanomaterials on the rutting resistance of bitumen (Yao et al., 2013a). In summary, it is concluded that

the anti-ageing compounds B (Irganox acid), D (Irganox acid:furfural) and F (DLTDP:Irganox acid:furfural) reduce the rutting resistance of the bitumen samples that is not significantly changed by the formulations A (DLTDP:furfural), C (NaMMT:Irganox acid) and E (NaMMT:Irganox acid:furfural).

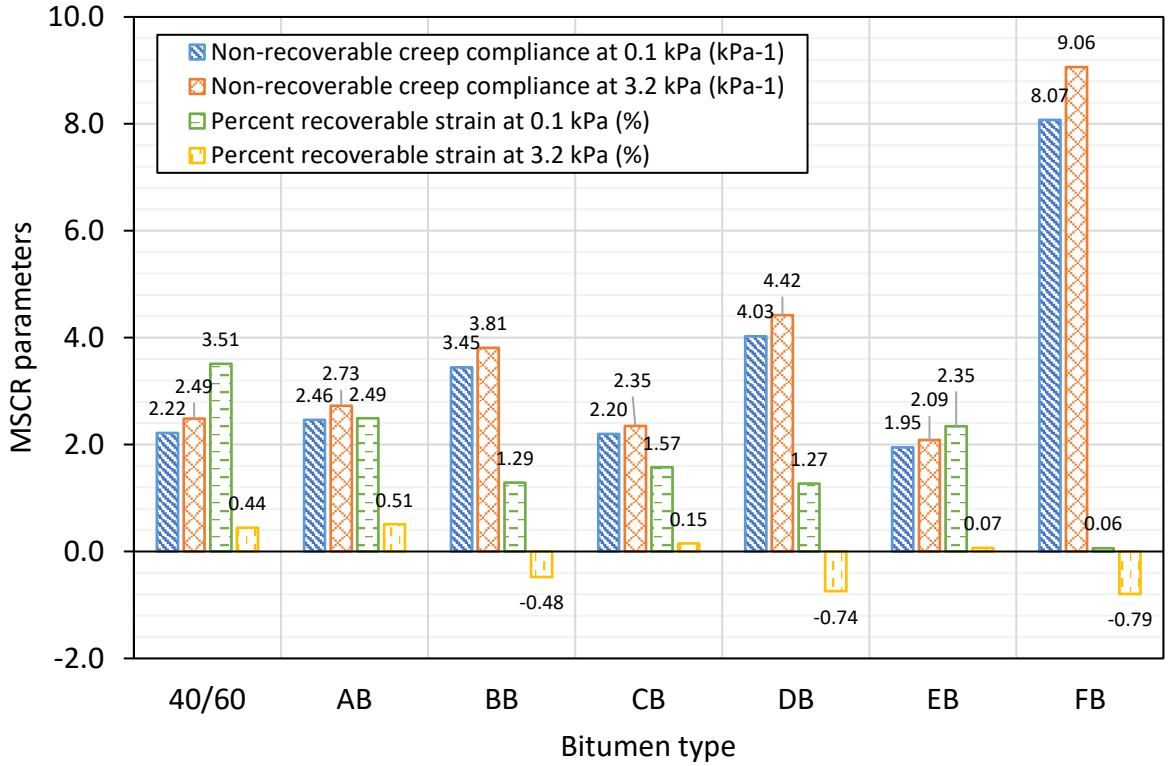


**Fig. 13.** MSCR parameters for all the RTFO aged samples.

## 4. Conclusions

In this study, the effects of anti-ageing compounds (AACs) on the rheological and mechanical properties of the bitumen were investigated using the Dynamic Shear Rheometer (DSR) tests. The anti-ageing performance of all the AACs was evaluated by Fourier Transform Infrared (FTIR) Spectroscopy test. All the AAC modified bitumen samples were examined by a series of rheological tests to analyse their complex viscosity, linear viscoelastic (LVE) properties, fatigue and rutting performances. The main findings from this research are as follows:

(1) All the AACs that contained Irganox acid, with the exception of the formulation NaMMT:Irganox acid:furfural (E), resulted in highly effective stabilisation of the bitumen substrate (anti-ageing performance); the presence of furfural in the AAC compositions, on the other hand, displayed adverse effects.
(2) All the AAC modified bitumen samples exhibited a non-Newtonian behaviour. Irganox acid is shown to enhance the complex viscosity of the bitumen while the furfural reduces the viscosity.
(3) The unaged and 20-hour PAV-aged bitumen samples modified by the AACs can be considered as thermo-rheologically simple materials. The black diagram of the unaged sample FB with the formulation F (DLTDP:Irganox acid:furfural) showed an inverse ‘‘C’’ pattern, which is significantly different from that of the remaining AAC modified bitumen samples.
(4) The samples BB with Irganox acid and CB with NaMMT:Irganox acid are somewhat stiffer than the control sample 40/60 due to the presence of a high concentration (10%) of Irganox acid. However, the samples AB (with DLTDP:furfural), DB (with Irganox acid:furfural), EB (with NaMMT:Irganox

acid:furfural) and FB (with DLTDP:Irganox acid:furfural) became softer because of the addition of the furfural.

(5) The anti-ageing compounds A (DLTDP:furfural), D (Irganox acid:furfural) and F (DLTDP:Irganox acid:furfural) have significantly strengthened the resistance of the bitumen samples to fatigue cracking.

(6) NaMMT enhanced the rutting resistance of bitumen samples while Irganox acid and furfural weakened the rutting performance of the samples.

This study evaluated the oxidative stability (anti-ageing), rheological and mechanical performances of bitumen modified with different anti-ageing compounds (AACs). Future study will be continued to investigate the low temperature performance of the AAC-modified bitumen. In addition, different base bitumen will be examined to further evaluate the influence of the AACs on the rheological and mechanical performances of bitumen.

## Conflict of interest

The authors declare that there are no conflicts of interest.

## Acknowledgement

The authors would like to acknowledge the support from the PPP Research Unit, CEAC, Aston University, UK. This work is part of a project that has received funding from the European Union's Horizon 2020 research and innovation programme under the Marie Skłodowska-Curie grant agreement No 101030767.

## References

Airey, G.D., 2002. Use of black diagrams to identify inconsistencies in rheological data. Road Materials and Pavement Design 3(4), 403-424.

Airey, G.D., Brown, S.F., 1998. Rheological performance of aged polymer modified bitumens. Journal of the Association of Asphalt Paving Technologists 67.

Apeagyei, A.K., 2006. Development of antioxidant treatments for asphalt binders and mixtures. University of Illinois at Urbana-Champaign.

Apeagyei, A.K., 2011. Laboratory evaluation of antioxidants for asphalt binders. Construction and Building Materials 25(1), 47-53.

ASTM, 2010. D 7405, Standard test method for multiple stress creep and recovery (MSCR) of asphalt binder using a dynamic shear rheometer. American Society for Testing and Materials, West Conshohocken, PA.

ASTM, 2012. D 2872, Standard test method for effect of heat and air on a moving film of asphalt (rolling thin-film oven test). American Society for Testing and Materials, West Conshohocken, PA.

ASTM, 2013. D 6521, Standard practice for accelerated aging of asphalt binder using a pressurized aging vessel (PAV). American Society for Testing and Materials, West Conshohocken, PA.

Cuciniello, G., Leandri, P., Polacco, G., Airey, G., Losa, M., 2020. Applicability of time-temperature superposition for laboratory-aged neat and SBS-modified bitumens. Construction and Building Materials 263, 120964.

Cui, Y., Glover, C.J., Braziunas, J., Sivilevicius, H., 2018. Further exploration of the pavement oxidation model–diffusion-reaction balance in asphalt. Construction and Building Materials 161, 132-140.

Ding, Y., Huang, B., Hu, W., Tang, B., Yu, M., 2019. Utilizing recycled asphalt shingle into pavement by extraction method. Journal of Cleaner Production 236, 117656.

Dintcheva, N.T., Al-Malaika, S., Morici, E., 2015. Novel organo-modifier for thermally-stable polymer-layered silicate nanocomposites. Polymer Degradation and Stability 122, 88-101.

Gao, Y., 2020. Multiscale Modelling of Bonding Performance of Bituminous Materials. Aston University.

Gao, Y., Li, L., Zhang, Y., 2020a. Modeling Crack Propagation in Bituminous Binders under a Rotational Shear Fatigue Load using Pseudo J-Integral Paris' Law. Transportation Research Record, 0361198119899151.

Gao, Y., Li, L., Zhang, Y., 2020b. Modelling crack initiation in bituminous binders under a rotational shear fatigue load. International Journal of Fatigue 139, 105738.

Gao, Y., Zhang, Y., Gu, F., Xu, T., Wang, H., 2018. Impact of minerals and water on bitumen-mineral adhesion and debonding behaviours using molecular dynamics simulations. Construction and Building Materials 171, 214-222.

Gao, Y., Zhang, Y., Yang, Y., Zhang, J., Gu, F., 2019. Molecular dynamics investigation of interfacial adhesion between oxidised bitumen and mineral surfaces. Applied Surface Science 479, 449-462.

Gawel, I., Czechowski, F., Kosno, J., 2016. An environmental friendly anti-ageing additive to bitumen. Construction and Building Materials 110, 42-47.

Glover, C.J., Martin, A.E., Chowdhury, A., Han, R., Prapaitrakul, N., Jin, X., Lawrence, J., 2009. Evaluation of binder aging and its influence in aging of hot mix asphalt concrete: literature review and experimental design. Texas Transportation Institute.

Herrington, P.R., 2012. Diffusion and reaction of oxygen in bitumen films. Fuel 94, 86-92.

Hou, X., Lv, S., Chen, Z., Xiao, F., 2018. Applications of Fourier transform infrared spectroscopy technologies on asphalt materials. Measurement 121, 304-316.

Karnati, S.R., Oldham, D., Fini, E.H., Zhang, L., 2019. Surface functionalization of silica nanoparticles to enhance aging resistance of asphalt binder. Construction and Building Materials 211, 1065-1072.

Lamontagne, J., Dumas, P., Mouillet, V., Kister, J., 2001. Comparison by Fourier transform infrared (FTIR) spectroscopy of different ageing techniques: application to road bitumens. Fuel 80(4), 483-488.

Li, L., Gao, Y., Zhang, Y., 2020. Crack length based healing characterisation of bitumen at different levels of cracking damage. Journal of Cleaner Production 258, 120709.

Liu, H., Zhang, H., Hao, P., Zhu, C., 2015. The effect of surface modifiers on ultraviolet aging properties of nano-zinc oxide modified bitumen. Petroleum Science and Technology 33(1), 72-78.

Omairey, E.L., Gu, F., Zhang, Y., 2021. An equation-based multiphysics modelling framework for oxidative ageing of asphalt pavements. Journal of Cleaner Production 280, 124401.

Omairey, E.L., Zhang, Y., Al-Malaika, S., Sheena, H., Gu, F., 2019. Impact of anti-ageing compounds on oxidation ageing kinetics of bitumen by infrared spectroscopy analysis. Construction and Building Materials 223, 755-764.

Omairey, E.L., Zhang, Y., Gu, F., Ma, T., Hu, P., Luo, R., 2020. Rheological and fatigue characterisation of bitumen modified by anti-ageing compounds. Construction and Building Materials 265, 120307.

Petersen, J.C., Glaser, R., 2011. Asphalt oxidation mechanisms and the role of oxidation products on age hardening revisited. Road Materials and Pavement Design 12(4), 795-819.

Petersen, J.C., Harnsberger, P.M., 1998. Asphalt aging: dual oxidation mechanism and its interrelationships with asphalt composition and oxidative age hardening. Transportation Research Record 1638(1), 47-55.

Tang, N., Huang, W., Hu, J., Xiao, F., 2018. Rheological characterisation of terminal blend rubberised asphalt binder containing polymeric additive and sulphur. Road Materials and Pavement Design 19(6), 1288-1300.

577 Wang, H., Liu, X., Apostolidis, P., Scarpas, T., 2018. Rheological behavior and its chemical interpretation
578 of crumb rubber modified asphalt containing warm-mix additives. Transportation Research Record
579 2672(28), 337-348.

580 Xu, G., Wang, H., Zhu, H., 2017. Rheological properties and anti-aging performance of asphalt binder
581 modified with wood lignin. Construction and Building Materials 151, 801-808.

582 Yao, H., You, Z., Li, L., Goh, S.W., Lee, C.H., Yap, Y.K., Shi, X., 2013a. Rheological properties and
583 chemical analysis of nanoclay and carbon microfiber modified asphalt with Fourier transform infrared
584 spectroscopy. Construction and Building Materials 38, 327-337.

585 Yao, H., You, Z., Li, L., Lee, C.H., Wingard, D., Yap, Y.K., Shi, X., Goh, S.W., 2013b. Rheological
586 properties and chemical bonding of asphalt modified with nanosilica. Journal of Materials in Civil
587 Engineering 25(11), 1619-1630.

588 You, Z., Mills-Beale, J., Foley, J.M., Roy, S., Odegard, G.M., Dai, Q., Goh, S.W., 2011. Nanoclay-
589 modified asphalt materials: Preparation and characterization. Construction and Building Materials 25(2),
590 1072-1078.

591 Yusoff, N.I.M., Jakarni, F.M., Nguyen, V.H., Hainin, M.R., Airey, G.D., 2013. Modelling the rheological
592 properties of bituminous binders using mathematical equations. Construction and Building Materials 40,
593 174-188.

594 Zhang, Y., Birgisson, B., Lytton, R.L., 2016. Weak form equation–based finite-element modeling of
595 viscoelastic asphalt mixtures. Journal of Materials in Civil Engineering 28(2), 04015115.

596 Zhang, Y., Gao, Y., 2019. Predicting crack growth in viscoelastic bitumen under a rotational shear fatigue
597 load. Road Materials and Pavement Design, 1-20.

598